J. Fluid Mech. (1985), *vol.* 158, *pp.* 245–268
Printed in Great Britain

Numerical simulation of the turbulent Rayleigh–Bénard problem using subgrid modelling

By THOMAS M. EIDSON
Georgia Institute of Technology, School of Mechanical Engineering

(Received 27 June 1984 and in revised form 18 December 1984)

A numerical simulation of turbulent natural convection (the Rayleigh–Bénard problem) has been conducted using large-eddy-simulation (LES) methods and the results compared with several experiments. The development of the LES equation is outlined and discussed. The modelling of the small-scale turbulent motion (called subgrid modelling) is also discussed. The resulting LES equations are solved and data collected over a short period of time in a similar manner to the direct simulation of the governing conservation equations. An explicit, second-order accurate, finite-difference scheme is used to solve the equations. Various average properties of the resulting flow field are calculated from the data and compared with experimental data in the literature. The use of a subgrid model allows a higher value of Ra to be simulated than was previously possible with a direct simulation. The highest Ra successfully simulated was 2.5×10^6. The problems at higher values of Ra are discussed and suggestions for improvements made.

1. Introduction

Calculation of turbulent fluid flows is complicated by the large range of scales that exist in these flows. Direct simulations of these equations (the Navier–Stokes equations and the energy equation for convective heat flows) is not possible for highly turbulent flows with foreseeable computers owing to the large core size and computation time required. The large-scale-averaging approach, where correlation terms (i.e. the Reynolds stresses) are modelled, is not always satisfactory because the physics of the various scales that contribute to the correlation terms is not the same. Thus, a simple model to incorporate both the large- and small-scale physics is a difficult task. Even solving differential equations for the correlation terms does not solve this fundamental problem.

The large-eddy-simulation technique (LES) overcomes some of these difficulties. A set of filtered flow equations can be formed by filtering the original flow equations (the Navier–Stokes and other pertinent transport equations) with different filter widths. The procedure is discussed by Kwak (1975) and Shaanan (1975) for spacial averaging. The set is parametrized by the filter width and ranges from the original flow equations (zero filter width) to the mean-flow turbulent equations (very large filter width). By selecting the filter width Δ_f approximately equal to the size of the numerical grid width Δ one attains the equations to be solved using the LES technique. Reynolds (1976), Herring (1979) and Rogollo & Moin (1984) have surveyed some of the early work in this area. Though all researchers do not use the filter concept, the essence of their approach is the same (Deardorff 1973; Schumann, Grotzbach & Kleiser 1980).

The LES flow equations are similar to the original flow equations with the inclusion of the correlation terms – the predominant ones being a term similar to the Reynolds stress and a velocity–temperature correlation term in the energy equation. Solutions to the LES equations are also similar but the small-scale fluctuations (smaller than Δ_f) have been implicitly removed. The LES correlation terms which must be modelled or measured now contain only the small-scale turbulence. The small-scale motion is independent of the boundary conditions and can be modelled as a function of local flow conditions. This is an easier task than modelling both the small- and large-scale turbulent physics together. Since the correlation terms contain only a modelled estimate of the average effect of the small scales, the resulting solutions are therefore model estimates of the true solutions to the Navier–Stokes equations.

The study of thermal turbulence is a problem for which the LES approach is particularly useful. Experimental data concerning the flow details are difficult to attain, especially when the mean velocity is zero. Long-time-average correlations of velocity and temperature, which quantify the heat-transfer physics, are dependent on the boundary conditions and are difficult to model (Long 1976, 1977). The LES approach is a natural choice for further study of thermal turbulence since this method provides a more detailed evaluation of the correlation terms. Deardorff (1973) has previously used this method to study atmospheric flows driven by thermal convection. The turbulent Rayleigh–Bénard problem was selected for study using the LES approach since it is a simple, documented problem that contains the natural-convection physics. Grotzbach (1982) and Lipps (1976) have performed similar calculations for the Rayleigh–Bénard problem. They did not include subgrid modelling and were limited to an *Ra* which was an order of magnitude smaller than this study. The choice of a problem uncomplicated by additional physical phenomena, and of using only the basic LES concepts of a filtered average and the algebraic equation modelling of the resulting Reynolds stress-like terms, was made to make the evaluation of the coupling of the problem and the solution technique clearer. Several refinements to the basic LES theory have been tested on other flows (principally, homogeneous box turbulence). These were purposely left out since the advantages and disadvantages of these modifications have not been fully studied (Moin *et al.* 1978; Mansour *et al.* 1979; Antonopoulos-Domis 1979).

2. Rayleigh–Bénard problem

2.1. *Problem definition*

The study of the heat transfer across an infinite, horizontal fluid layer heated from below and the resulting fluid motion has been used by many researchers to understand the fundamentals of natural convection. The basic geometry and physical parameters are shown in figure 1. The bottom plate is maintained at a higher temperature than the top plate, resulting in either conductive or convective heat transfer. The temperature of each plate is kept uniform in the horizontal directions and constant in time. Several modifications of the above have also been studied. For laboratory experimental studies and numerical simulations, the horizontal dimension must be finite. The problem is also studied with the zero-velocity boundary conditions of one or both flat plates replaced by zero-stress boundary conditions associated with a free boundary. A basic description of the Rayleigh–Bénard problem is given by Chandrasekhar (1961). Later articles by Busse (1981), Long (1977) and Denton & Wood (1979) survey more recent work on the problem. The case of flate-plate

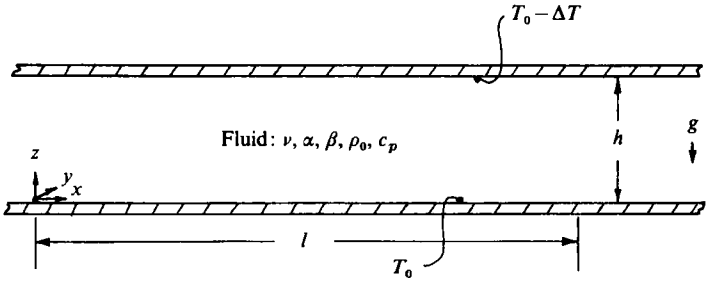

FIGURE 1. Geometry and parameters of the Rayleigh–Bénard problem.

boundaries with finite horizontal dimensions is the subject in this study. The basic study is limited to the region where the fluid motion is turbulent, $Ra \geqslant 10^5$. The results from a preliminary study at $Ra = 10^4$ are also presented.

2.2. *Differential equations*

The governing equations for the fluid layer are the usual balance equations for conservation of mass, momentum and energy. The Boussinesq approximation is employed to simplify the mathematical analysis (Spiegel & Veronis 1960; Mihaljan 1962). The dependent variables of the problem – $\hat{u}_i$ (or $\hat{u}$, $\hat{v}$, $\hat{w}$), $\hat{T}_a$ and $\hat{P}_a$ – are respectively the three velocity components, the temperature and the pressure. $\hat{x}_i$ (or $\hat{x}$, $\hat{y}$, $\hat{z}$) and $\hat{t}$ are the spacial Cartesian co-ordinates and time. $i = 1$ and 2 signifies the horizontal direction and $i = 3$ gives the vertical direction perpendicular to the plate boundaries. The fluid properties and problem parameters are as follows: ρ is the fluid density, ρ_0 is the fluid density at the reference temperature, ν is the kinematic viscosity, α is the thermal diffusivity, β is the coefficient of thermal expansion, c_p is the specific heat, g is the acceleration of gravity, T_0 is the reference temperature which is the fluid lower-surface temperature, ΔT is the temperature difference between the upper and lower surfaces, and h is the distance between the upper and lower surfaces.

In order to simplify the computations, the temperature and vertical pressure gradient are split into three parts: (i) a constant reference term; (ii) a term based on a conductive temperature profile; and (iii) the perturbations owing to the convective velocities. The first two parts are analytically solved, leaving the perturbation quantities to be solved by the computer model:

$$\hat{T}_a(\hat{x}_k, \hat{t}) = T_0 - \frac{\Delta T}{h}\hat{x}_3 + \hat{T}(\hat{x}_k, t); \tag{1a}$$

$$\frac{\partial \hat{P}_a(x_k, \hat{t})}{\partial \hat{x}_3} = -\rho_0 g - \rho_0 g\beta \frac{\Delta T}{h}\hat{x}_3 + \frac{\partial \hat{P}(\hat{x}_k, \hat{t})}{\partial \hat{x}_3}. \tag{1b}$$

The convective-flow equations result from inserting (1 *a*, *b*) into the dimensional form of the governing equations and using α, h, ΔT and ρ_0 to obtain the following non-dimensional form:

$$\frac{\partial u_i}{\partial t} + \frac{\partial (u_i u_j)}{\partial x_j} = -\frac{\partial P}{\partial x_i} + Pr\frac{\partial^2 u_i}{\partial x_j^2} + Pr\, Ra\, T\delta_{i3}, \tag{2a}$$

$$\frac{\partial T}{\partial t} + \frac{\partial (T u_j)}{\partial x_j} = \frac{\partial^2 T}{\partial x_j^2} + u_3, \tag{2b}$$

and
$$\frac{\partial u_j}{\partial x_j} = 0. \tag{2c}$$

The non-dimensional form of the problem variables are represented using the same symbol as the dimensional form but with the (^) removed.

2.3. *Non-dimensional parameters and estimates*

Dimensional reasoning gives the heat transfer and fluid motion, in non-dimensional form: $Nu = q/(\alpha/h)\,\Delta T$ is the Nusselt number, $Pe = hU_{\text{r.m.s.}}/\alpha$ is the Péclet number, $Re = hU_{\text{r.m.s.}}/\nu$ is the Reynolds number. Nu and Pe or Re depend on the problem parameters grouped into two dimensionless numbers: $Ra = g\beta\,\Delta T h^3/\nu\alpha$, the Rayleigh number, and $Pr = \nu/\alpha$, the Prandtl number. q is the heat-transfer rate per unit area through the fluid layer divided by $\rho_0 c_p$ and $U_{\text{r.m.s.}}$ is the root mean square of a velocity fluctuation. Re and Pe can be defined for various averages of the different velocity components, collectively or individually. Krishnamurti (1970*a*, *b*) has mapped the regions of Ra and Pr where the resulting fluid motion and heat transfer are qualitatively different. For finite size in the horizontal direction a third parameter, the aspect ratio $A = l/h$, is needed. Here l is an imposed horizontal dimension. There should exist a characteristic horizontal dimension l_c which is a function of Ra and Pr. However, if A is much larger than $A_c = l_c/h$, then A should not be important.

Dimensional analysis can be used to suggest forms for Pe or Re (Businger 1973). These equations are only used for comparing the model output and estimating the time step and are not an assumption in the calculations. For turbulent flows, the important governing parameters are $g\beta$, $\overline{wT}$, h and ΔT. Both the heat transfer $\overline{wT}$ and ΔT cannot be independent. If ΔT is assumed independent, then a characteristic velocity can be defined as follows:
$$W_c = (g\beta\,\Delta T\, h)^{\frac{1}{2}}, \tag{3}$$

or
$$Pe = \frac{hW_c}{\alpha} = (Ra\,Pr)^{\frac{1}{2}}. \tag{4}$$

Similarly the heat input at the boundary q can be assumed independent. Since $q = \overline{wT}$ away from the wall,
$$W_c = (g\beta h\overline{wT})^{\frac{1}{3}}, \tag{5}$$

or
$$Pe = (Pr\,Ra\,Nu)^{\frac{1}{3}}. \tag{6}$$

An equivalent relation to (5) for a characteristic temperature can be derived as follows:
$$\frac{T_c}{\Delta T} = \left(\frac{Nu^2}{Ra\,Pr}\right)^{\frac{1}{3}}. \tag{7}$$

T_c and W_c have been found experimentally to scale the r.m.s. temperature and velocity levels as Ra is varied (Deardorff 1970*b*). No experimental study is known that shows whether (4) or (6) is better. Note that $(Ra\,Nu)^{\frac{1}{3}}$ is approximately $Ra^{\frac{4}{9}}$ assuming $Nu \sim Ra^{\frac{1}{3}}$; thus the exponents of the two equations are not greatly different.

2.4. *Boundary region*

As with the boundary-layer concept in isothermal flows, the flow near the wall boundary can be treated differently from the flow away from it to attain a more efficient model. The core region is composed of a flow field for which the small-scale motion is isotropic and in a state of equilibrium, as defined by Kolmogoroff's theory.

The flow in this region satisfies, for large Ra, the assumptions of subgrid modelling to be discussed in §4. At the lower Ra values of this study a large equilibrium region does not exist and this assumption is violated. However, at the lower values of Ra, only a small fraction of the turbulent motions are modelled. Near the wall the character of the turbulence is different; for example, the long-time-average turbulent production, dissipation, and diffusion vary significantly as a function of the distance from the wall (Deardorff & Willis 1967). Modelling of the long-time-average correlation terms for the near-wall region is not fully understood because only limited data are available. Modelling of the subgrid correlation terms that result in the LES approach has no known direct, experimental support. The core subgrid model has indirect support through previous LES studies, but little work has been done in the wall area (especially for natural convection) (Moin & Kim 1982). No experimental evidence exists to show how the subgrid turbulence near the wall differs from the core subgrid turbulence. However, the lengthscale of a subgrid model is expected to be reduced to account for the reduction in typical eddy sizes owing to the nearness of the wall. Thus, one possibility is to use the core-region subgrid model with the lengthscale reduced in the wall region.

Another approach is to modify the subgrid model to account for direct production of turbulence caused by buoyancy at the subgrid level. In a natural-convection flow the production and other correlation terms of the turbulence can be modelled as a function of the gradient of the filtered temperature as well as of velocity. For a long-time average the mean velocity and thus its spacial gradients are zero. Therefore the turbulent production, r.m.s. velocity, and other mean correlation terms can be modelled only with the mean temperature gradient. For a filtered velocity and temperature field the instantaneous, spacial gradients are non-zero. The subgrid turbulence is assumed to be a function of the next-higher scales (due to the physics of cascading) and can thus be modelled by the local filtered velocity and/or temperature fields. Production of the subgrid turbulence by the filtered velocity gradient seems well justified, but direct production owing to buoyancy is not obvious. First, define a local Rayleigh and Reynolds number, $Ra_s \propto \Delta T_s h_s^3$ and $Re_s \propto \Delta U_s h_s$ ($h_s, \Delta T_s$, and ΔU_s are the appropriate length, temperature and velocity scales that control the production of turbulence smaller than h_s). The production of turbulence with scales smaller than h_s (or cascading of turbulence) in general can be buoyancy generated as well as vorticity generated. However, because of the h_s^3 dependency, the buoyancy generation should be less than the vorticity generation for small h_s. This assumes ΔT_s and ΔU_s have similar variations with h_s. Near the wall this may not be true since the mean gradients are larger; thus ΔT_s could be large enough to cause a generation of subgrid motion owing to buoyancy. In short, inclusion of the production term owing to buoyancy in a subgrid correlation model is of more importance near the wall.

The final modelling problem near the wall is the handling of the viscous/conductive sublayer. If the numerical grid is not fine enough, a law of the wall must be used to account for the large curvature in velocity and temperature fields near the wall. No suitable law-of-the-wall theory is available for the mean flow field, much less for the filtered flow field.† Since it was desired to keep the grid uniform for simplicity and

† Several laws of the wall have been suggested: for example, $\bar{T} \propto z^{\frac{1}{7}}$ or $\bar{T} \propto z^{-1}$. However, the experimental data does not support any particular model (Businger 1973; Fitzjarrald 1976; Goldstein & Chu 1967; and Chu & Goldstein 1973). The existence of several sublayers with different dominant physics (Long 1976, 1977) suggests that a simple, universal law of the wall is not likely to exist.

not to use a law of the wall, the grid size had to be fine enough to include at least one point in the sublayer. The range of application of the overall model is limited by this assumption. As the Ra increases, the sublayer becomes smaller compared with the grid size and the model is no longer valid.

3. Large-eddy-simulation flow equations

The LES equations are formed by convolution-averaging (2) with a low-pass filter. $r = \Delta_f/\Delta$ typically varies from 1 to 2 with values up to 4 used in some studies (McMillan & Ferziger 1979). The convolution average is defined as follows:

$$\bar{u}^f(x_k, t) = \int_{-\infty}^{\infty} G(x_k - x_k')\, u(x_k', t)\, \mathrm{d}x_k', \tag{8a}$$

$$\int_{-\infty}^{\infty} G(x_k')\, \mathrm{d}x_k' = 1. \tag{8b}$$

The effects of different choices for G (other than being a low-pass filter of appropriate width) manifest themselves only when the higher-order correlation terms are considered. Here, these are neglected and so the choice of the following form for G is not critical to this study:

$$G(x_k - x_k') = \begin{cases} \dfrac{1}{\Delta_f} & \text{for } |x_k - x_k'| < \tfrac{1}{2}\Delta_f, \\ 0 & \text{for } |x_k - x_k'| \geqslant \tfrac{1}{2}\Delta_f, \end{cases} \tag{9a}$$

$$\Delta_f = \Delta. \tag{9b}$$

Kwak (1975) and Shaanan (1975) discuss the various properties of this average, two of which should be noted. First, it is commutable with the derivative operators and therefore can be applied to the flow equations with results similar to the long-time average. The second property is that it allows for scale information of order $1/\Delta_f$ to be included in the filtered flow equations in a direct manner. This is accomplished when the dependent variables ($u_i(x_k, t)$ and $T(x_k, t)$) are split into a filtered term ($^{-f}$) and a fluctuating or small-scale term $(\ )'^f$ similar to the Reynolds splitting using long-time averages:

$$u_i(x_k, t) = \bar{u}_i^f(x_k, t) + u_i'^f(x_k, t); \tag{10a}$$

$$T(x_k, t) = \bar{T}^f(x_k, t) + T'^f(x_k, t). \tag{10b}$$

Equations (2a, b, c) can be filtered using (8a, b) and (9a, b). Equations (10a, b) are then inserted. Several higher-order terms can be neglected and these are discussed in Rogallo & Moin (1984), Antonopoulos-Domis (1979) and Clark, Fertziger & Reynolds (1979). This averaging results in two terms, $\overline{u_i'^f u_j'^f}^f$ and $\overline{u_j'^f T'^f}^f$, which are similar to the conventional Reynolds stresses. They must be modelled and this is discussed in §4. Equations (2a, b, c) now become

$$\frac{\partial \bar{u}_i^f}{\partial t} + \frac{\partial(\bar{u}_i^f \bar{u}_j^f)}{\partial x_j} = -\frac{\partial \bar{P}^f}{\partial x_i} + Pr\, Ra\, \bar{T}^f \delta_{i3} + Pr \frac{\partial^2 \bar{u}_i^f}{\partial x_j^2} - \frac{\partial(\overline{u_i'^f u_j'^f}^f)}{\partial x_j}, \tag{11a}$$

$$\frac{\partial \bar{T}^f}{\partial t} + \frac{\partial(\bar{T}^f \bar{u}_j^f)}{\partial x_j} = \frac{\partial^2 \bar{T}^f}{\partial x_j^2} + \bar{u}_3^f - \frac{\partial(\overline{T'^f u_j'^f}^f)}{\partial x_j}, \tag{11b}$$

$$D = \frac{\partial \bar{u}_j^f}{\partial x_j} = 0. \tag{11c}$$

A Poisson equation is used in place of (11*c*):

$$\frac{\partial^2 \bar{P}^{\mathrm{f}}}{\partial x_j^2} = \frac{\partial G_j}{\partial x_j} + \frac{\partial D}{\partial t}. \tag{11d}$$

G_i (and G_T) are shorthand notations, defined by comparing (11*a*, *b*) to the following equations:

$$\frac{\partial \bar{u}_i^{\mathrm{f}}}{\partial t} + \frac{\partial \bar{P}^{\mathrm{f}}}{\partial x_j} = G_i, \quad i = 1, 2, 3, \tag{12a}$$

$$\frac{\partial \bar{T}^{\mathrm{f}}}{\partial t} = G_T. \tag{12b}$$

D is in general zero but is included in (11*d*) for numerical-stability reasons.

4. Modelling of the subgrid correlation terms

4.1. *Model derivations*

The subgrid theory has been documented by Reynolds (1976), Schumann *et al.* (1980), Eidson (1982) and Rogollo & Moin (1984). For the reasons discussed in the preceding sections, essentially the same model for the subgrid turbulence has been used by various researchers for a wide range of boundary conditions. A modification (Lilly 1962), outlined below and used in this study, allows for the production of subgrid turbulence owing to buoyancy caused by temperature gradients in the large-scale or filtered flow field. Limited tests showed a small improvement in the r.m.s. levels in the wall regions with the buoyancy term included and it was therefore included in the subgrid modelled for the simulations reported in this paper (Eidson 1982). A more thorough study of the buoyancy-production correction is needed, however.

$u_i'^{\mathrm{f}} u_j'^{\mathrm{f}}$ can be interpreted as a stress similar to $\overline{u_i' u_j'}$ (the Reynolds stress). Similar dimensional and production–dissipation equilibrium arguments are used to develop a model for $u_i'^{\mathrm{f}} u_j'^{\mathrm{f}}$. However, for the LES case the subgrid turbulence is produced by the large-scale turbulence where the filter splits the two ranges somewhere in the Kolmogoroff equilibrium region. Since the subgroup turbulence is assumed isotropic, the velocity gradient used to model it should not have a preferred direction. The following form first suggested by Smagorinsky (1963) is generally used:

$$\overline{u_i'^{\mathrm{f}} u_j'^{\mathrm{f}}}^{\mathrm{f}} - \tfrac{1}{3}\delta_{ij}\overline{u_k'^{\mathrm{f}} u_k'^{\mathrm{f}}}^{\mathrm{f}} = -K\bar{S}_{ij}^{\mathrm{f}}; \tag{13a}$$

$$K = \frac{(C\Delta)^2}{\sqrt{2}}\bar{S}^{\mathrm{f}}; \tag{13b}$$

$$\bar{S}^{\mathrm{f}} = (\bar{S}_{ij}^{\mathrm{f}} \bar{S}_{ij}^{\mathrm{f}})^{\frac{1}{2}}; \tag{13c}$$

$$\bar{S}_{ij}^{\mathrm{f}} = \frac{\partial \bar{u}_i^{\mathrm{f}}}{\partial x_j} + \frac{\partial \bar{u}_j^{\mathrm{f}}}{\partial x_i}. \tag{13d}$$

Other modelling approaches have been tried in which extra differential equations for the subgrid correlation terms are solved (Schumann *et al.* 1980; and Deardorff 1973).

The modification to (13*a*, *b*, *c*, *d*) is derived by assuming that the subgrid turbulent production P_{SG} includes a buoyancy term,

$$P_{\mathrm{SG}} = \tfrac{1}{2}\tau_{ij}^{\mathrm{t}} \bar{S}_{ij}^{\mathrm{f}} + Pr\, Ra\, \delta_{i3}\overline{u_i'^{\mathrm{f}} T'^{\mathrm{f}}}^{\mathrm{f}}, \tag{14a}$$

where

$$\tau_{ij}^{\mathrm{t}} = -\overline{u_i'^{\mathrm{f}} u_j'^{\mathrm{f}}}^{\mathrm{f}} + \tfrac{1}{3}\delta_{ij}\overline{u_k'^{\mathrm{f}} u_k'^{\mathrm{f}}}^{\mathrm{f}}. \tag{14b}$$

Additional assumptions include equilibrium of the small-scale turbulence $P_{SG} = \epsilon$, and that τ_{ij}^{t} (and $u_i'^{f} T'^{f}$) are functions of ϵ, Δ and $\bar{S}_{ij}^{f}$ (and $\partial \bar{T}^{f}/\partial x_i$). Here ϵ denotes the turbulent dissipation rate. Thus

$$\tau_{ij}^{t} = \epsilon^{\frac{1}{3}} (C\Delta)^{\frac{4}{3}} \bar{S}_{ij}^{f} \tag{15a}$$

and

$$\overline{u_i'^{f} T'^{f}}^{f} = \frac{\epsilon^{\frac{1}{3}} (C\Delta)^{\frac{4}{3}}}{Pr_t} \frac{\partial \bar{T}^{f}}{\partial x_i}, \tag{15b}$$

where C and Pr_t (the subgrid turbulent Prandtl number) are proportionality constants. Equations (15a, b) can be put in an eddy viscosity/conductivity form. Then

$$\tau_{ij}^{t} = K_m \bar{S}_{ij}^{f}, \tag{16a}$$

$$\overline{u_i'^{f} T'^{f}}^{f} = -K_T \frac{\partial \bar{T}^{f}}{\partial x_i}, \tag{16b}$$

$$K_m = K = \epsilon^{\frac{1}{3}} (C\Delta)^{\frac{4}{3}} \tag{16c}$$

and

$$K_T = \frac{K}{Pr_t} \tag{16d}$$

Combining (14)–(16), the following equation for K results:

$$K = \frac{(C\Delta)^2}{2^{\frac{1}{2}}} \left(\bar{S}^{f2} - 2 \frac{Pr\, Ra}{Pr_t} \frac{\partial \bar{T}^{f}}{\partial x_3} \right)^{\frac{1}{2}}. \tag{17}$$

Equation (17) is similar to (13b) but K is enhanced for an unstable temperature gradient. Note that K^2 was constrained to be equal to zero when $\bar{S}^{f2} \simeq 0$ and $\partial T/\partial x_3 > 0$ occur locally. The model constants in (13b) and (17) were assumed to have the same value because of lack of information. The $\frac{1}{3}\delta_{ij} \overline{u_j'^{f} u_k'^{f}}^{f}$ term in (13a) is combined with the pressure when substituted into (11a) forming a pseudo-pressure which is calculated by the model. If the actual pressure is desired, $\frac{1}{3}\delta_{ij} \overline{u_k'^{f} u_k'^{f}}^{f}$ must be estimated (Deardorff 1972).

4.2. *Model constants*

The model constant C in (13b) has been fairly well established. Values of C from several numerical studies as well as several theoretical estimates by Lilly (Deardorff 1971) are shown in table 1. A value of $C = 0.21$ was selected for this study since the work of Deardorff (1972) most nearly matched the boundary conditions of this study.

The subgrid turbulent Prandtl number Pr_t having different physical significance, does not have the value obtained for long-time-averaged turbulence. Studies by Grotzbach (1980), Grotzbach & Schumann (1979) and Deardorff (1971, 1972) suggest a range of $\frac{1}{2}$ to $\frac{1}{3}$. This is at the low end of the values surveyed by Reynolds (1975) for long-time-averaged turbulence. A value of 1/2.5 was selected for this study.

5. Finite-difference scheme

A simple, but previously well tested, numerical scheme was chosen. The main feature of this scheme was that it had minimum numerical diffusion with good stability properties. The second-order, explicit, finite-difference scheme discussed by Williams (1969) was used. It is a leapfrog scheme with a lagged diffusion term. The

C	Source
Isotropic box turbulence	
0.17–0.19	Clark (1979)
0.14–0.16	McMillan & Ferziger (1979)
0.21	Kwak (1975)
0.24	Shaanan (1975)
0.19–0.24	Mansour *et al.* (1979)
Atmospheric convection	
0.21 (unstable $\partial T/\partial z$)	Deardorff (1972)
0.13 (neutral $\partial T/\partial z$)	Deardorff (1972)
Channel flow	
0.10	Deardorff (1970*a*)
Theory	
0.18–0.22 (Estimates by Lilly)	Deardorff (1971)

TABLE 1. Value of C from several studies

Computer	CRAY1, located at the National Center for Atmospheric Research Facility in Boulder, Colorado
Core requirements	approximately 1 megaword for program code and variable storage (99% of CRAY1 core)
Array size	1. 69696 grid points 2. 10 main variables – u, v, w, t, at 2 time steps; P and Q 3. 696960 storage locations for main variables
Time requirements	1. 0.67 s per time step 2. 1000 s per run (1500 time steps)

TABLE 2. Computational statistics

momentum term was modified as suggested by Piacsek & Williams (1970). A time filter suggested by Robert (1966) was used to prevent time splitting. The $\partial D/\partial t$ correction to prevent nonlinear instabilities was noted in §3. The dependent variables were staggered on the numerical grid as in Williams (1969). The numerical grid had equal values of Δ in the three coordinate directions.

Periodic boundary conditions were assumed in the horizontal direction. A large aspect ratio is desired to minimize the effect of these mathematical boundary conditions. A minimum of $A = 3$ (with 8–10 suggested) is necessary to include the largest natural wavelengths, based on the work of Deardorff & Willis (1965) and Fitzjarrald (1976). A value of $A = 4$ was used for this study, being the largest that the computer could accommodate without large input/output cost, table 2. The effects of A are also discussed by Grotzbach (1982, 1983).

No-slip boundary conditions were used at the top and bottom walls and the temperature of the wall and the fluid were assumed to be the same. As discussed in §2, the viscous/conductive sublayer must be thick enough for the numerical scheme to determine accurately the derivatives near the wall. This is the weakest assumption in the overall model and was the probable reason for the lack of success of the model at high Ra.

The computational statistics are shown in table 2.

6. Results of numerical simulation

6.1. *Ra variation*

As the primary goal of this study was to evaluate the LES approach to studying turbulent natural convection, the model was run at 6 turbulent Rayleigh numbers ($Pr = 0.71$) and compared with experimental data reported in the literature. The simulations were started with a zero velocity field and a random temperature field. The random field was calculated from zero mean white noise with a small variance. The simulations were run for approximately 500 time steps to develop a 'steady' turbulent flow. 1000 additional steps were run to collect data for analysis. A time step of $\Delta_t = 0.17\Delta/W_c$ was used where the largest velocity flow scales were estimated from (5). This relation was determined from a von Newman stability analysis of the basic scheme and the coefficient was increased slightly based on scaled-down ($A = 1$) tests of the model (Eidson 1982).

The filtered flow fields resulting from the model were assumed to be horizontally homogeneous and statistically steady in time. The long-'term' averages to be compared with the experimental results in the literature were both horizontally and time averaged. These averages are denoted by $\langle\ \rangle$. The total long-'term' averages included a filtered-field component and a subgrid-field component:

$$(u_i)_{\text{r.m.s.}} = (\langle u_i^2\rangle)^{\frac{1}{2}}; \tag{18a}$$

$$(u_i)^2_{\text{r.m.s.}} = \langle(\bar{u}_i^{\text{f}})^2\rangle + \langle(u_i'^{\text{f}})^2_{\text{r.m.s.}}\rangle. \tag{18b}$$

The subgrid term is estimated using (13a):

$$\langle(u_i'^{\text{f}})^2_{\text{r.m.s.}}\rangle = (\langle -K_m \bar{S}_{ii}^{\text{f}}\rangle + \tfrac{2}{3}\langle E_{\text{SG}}\rangle). \tag{19}$$

No summation is made on subscript i. E_{SG} is the subgrid kinetic energy and is estimated as (Lilly 1967)

$$E_{\text{SG}} = \int_{\pi/\Delta}^{\infty} E(k)\,\mathrm{d}k = \left(\frac{K}{0.094\Delta}\right)^2. \tag{20}$$

$E(k)$ is the kinetic energy transformed into wavenumber space k. A similar estimate for the subgrid temperature variance can be made (Shumann 1973). The Nu is calculated using

$$Nu = \frac{\partial\langle\bar{T}^{\text{f}}\rangle}{\partial x} + \langle wT\rangle \tag{21}$$

and

$$\langle wT\rangle = \langle\bar{w}^{\text{f}}\bar{T}^{\text{f}}\rangle + \langle\overline{w'^{\text{f}}T'^{\text{f}}}^{\text{f}}\rangle, \tag{22}$$

where $w'^{\text{f}}T'^{\text{f}^{\text{f}}}$ is estimated from (16b).

An important global result for comparison is the prediction of the Nu *versus* Ra relationship. Nu is formed from $\langle q\rangle$ near the vertical centre of the fluid: $\langle q\rangle$ was constant with vertical distance as is necessary for 'steady' conditions. Assuming the following form, the exponent a can be calculated from the simulation results, C_{Nu} being a constant:

$$Nu = C_{Nu}\,Ra^a. \tag{23}$$

Using the data from the 4 lowest Ra points in figure 2, $a = 0.28$. The model prediction of the exponent for this range ($Ra < 2.5 \times 10^6$) is in excellent agreement with several experimental results. The variation of repeat tests (using different starting fields) has been included as error bars in figure 2 (also in figures 4 and 5). The magnitude of Nu is higher than the experimental results, however. This is consistent with the direct

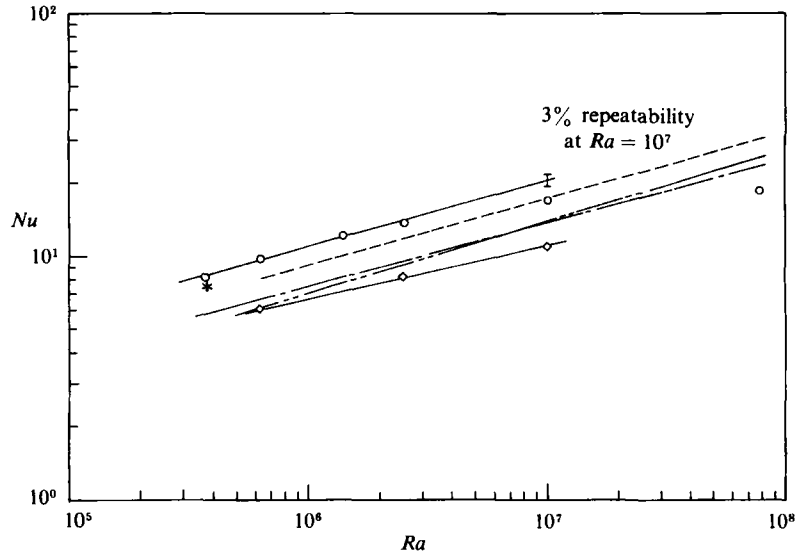

FIGURE 2. Comparison of the simulation model with experimental measurements, Nu *vs* Ra: $Nu = C_{Nu} Ra^a$. $a = 0.28$, O—O, model; —◇—, Deardorff & Willis (1967); $a = 0.294$, ---, Goldstein & Chu (1969); $a = 0.26$, —·—, Carrol (1976); $a = 0.30$, —··—, Fitzjarrald (1976); *, Grotzbach (1982).

simulations at lower, but still turbulent, Rayleigh numbers by Grotzbach (1982) and Lipps (1976). Grotzbach suggests that this is owing to the small aspect ratios used in the numerical simulations. Based on the work of Lipps & Sommerville (1971) and Fitzjarrald (1976), Grotzbach suggests that a large aspect ratio allows larger wavelength motions which impede the occurrence of heat flux. As a check on this hypothesis, the model was run using an aspect ratio of 2 and compared with the base-study results ($A = 4$). The increase in Nu from 13.8 ($A = 4$) to 14.4 ($A = 2$) for $Ra = 2.5 \times 10^6$ is small, but it shows the above trend. Another possibility is insufficient grid resolution near the wall. Comparison of cases 7, 8, and 9 with cases 13 and 14 in Grotzbach (1982) show a higher Nu for a larger grid. Grotzbach (1983) discusses this further.

Above $Ra = 2.5 \times 10^6$, the Nu values do not increase at the rate suggested by the experimental data. In fact, they appear to be asymptotically approaching a maximum level. An analysis of the heat-transfer boundary condition suggests a reason for the model's failure. The data of Goldstein & Chu (1969) in figure 3 show that for $Ra > 3 \times 10^6$ the first vertical grid point is outside the conductive sublayer δ (the region where $\overline{T}^{\mathrm{f}}$ or θ *versus* x_3 is linear). Thus for the larger values of Ra the grid resolution is not sufficient. The insufficient resolution can be shown to place a limit on the maximum Nu that the model can predict. The average heat transfer must be the same at all vertical levels. If the Nu_{w} (the Nu at the wall) has a maximum, the Nu of the entire model is limited. Nu_{w} is solely a function of conduction. The second-order, finite-difference scheme used in this study for $\partial \overline{T}^{\mathrm{f}}/\partial x_3$ results in the following equation for Nu_{w}:

$$Nu_{\mathrm{w}} = \frac{3T_1 - \frac{1}{3}T_2}{\Delta}. \tag{24}$$

T_1 and T_2 are the values of $\overline{T}^{\mathrm{f}}$ at the closest ($x_3 = \frac{1}{2}\Delta$) and second closest ($x_3 = \frac{3}{2}\Delta$) grid points to the wall. The maximum realistic value of T_1 and minimum realistic

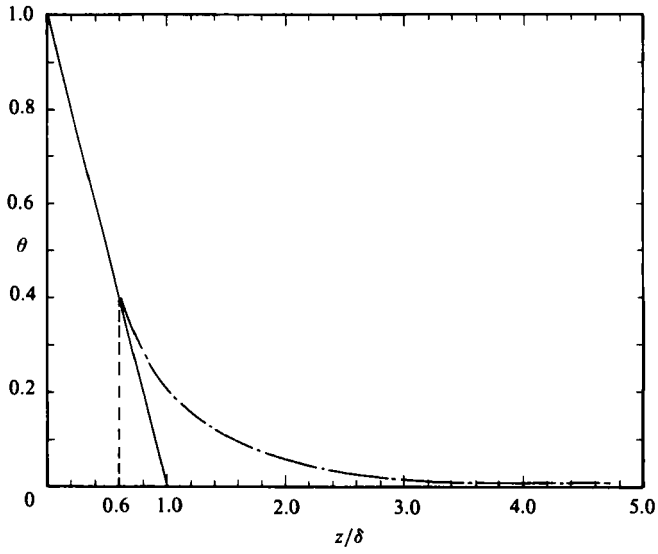

FIGURE 3. Estimate of conductive sublayer, data of Goldstein & Chu (1969), $6 \times 10^5 < Ra < 6 \times 10^6$: z_1, 1st grid point $= \frac{1}{32}$; $\delta_1 = z_1/(z/\delta)_1 = (\frac{1}{32})/0.6$; $Nu_1 = 1/2\delta_1 = 9.6$; $Nu = 0.123Ra^{0.294}$ $\Rightarrow Ra_1 \approx 3 \times 10^6$.

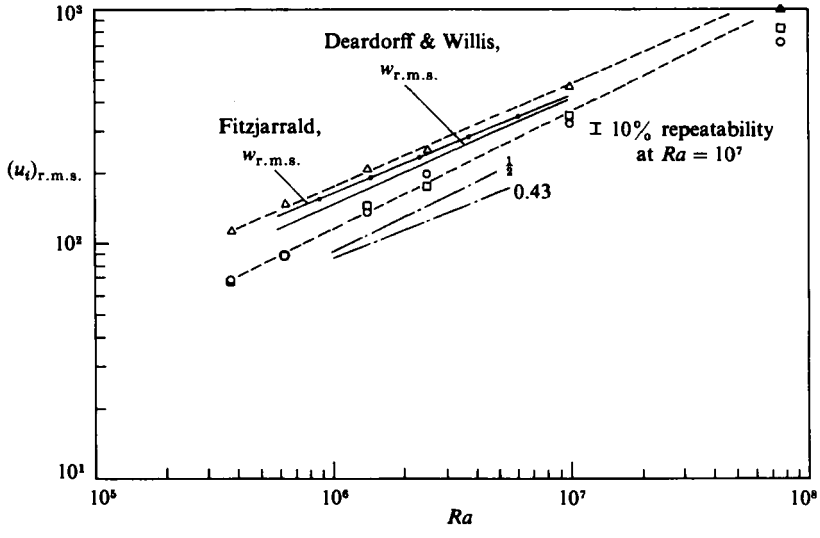

FIGURE 4. Comparison of the simulation model with experimental measurements, $(u_i)_{r.m.s.}$ *vs* Ra: △--△, $W_{r.m.s.}$; ○--○, $u_{r.m.s.}$ model; □--□, $v_{r.m.s.}$; —×—, dimensional estimates of slope (see §2.3); ——, experimental data.

value of T_2 are needed to maximize Nu_w. $T_1 = \frac{1}{2}$ and $T_2 = \frac{1}{2}$ give $(Nu_w)_{max} = 21$. Since the experimental values of Nu for Ra of order 10^7 are in the 15–20 range, the artificial cap on Nu by the model is a serious deficiency at the higher values of Ra.

The variation of the velocity and temperature r.m.s. levels as functions of Ra are shown in figures 4 and 5. Their comparison with experimental data is similar to the Nu results. They give good agreement with the power-law exponent predicted by dimensional arguments and measured by the experiments. However, their values are higher than the experimental measurements. The correlation coefficients (table 3)

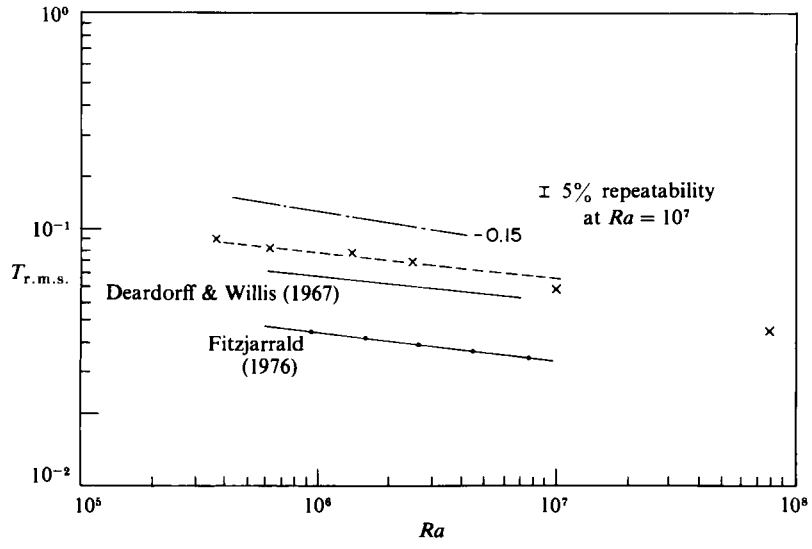

FIGURE 5. Comparison of the simulation model with experimental measurements, $T_{r.m.s.}$ *vs* Ra: ×--×, model; —⊖—, dimensional estimates of slope (see §2.3); ——, experimental data.

	C_{wT}			
Ra	Model	Deardorff & Willis (1967)	Fitzjarrald (1976)	Grotzbach (1981)
1.0×10^4	0.93	—	—	—
3.8×10^5	0.70	—	—	0.70
6.3×10^5	0.74	0.61	0.51	—
1.4×10^6	0.69	—	—	—
2.5×10^6	0.69	0.61	—	—
1.0×10^7	0.67	0.54	—	—

TABLE 3. Correlation coefficient of vertical velocity and temperature

predicted by the model are also high, so the high $\langle q \rangle$ away from the wall is not caused solely by the higher r.m.s. levels.

The vertical profiles of the horizontally averaged and time averaged temperature gave good agreement with the experimental data. In figure 6 the profile for $Ra = 6.3 \times 10^5$ is compared with the data of Deardorff & Willis (1967). Near the wall the model predicts a slightly larger slope, as is consistent with the higher value of Nu. Goldstein & Chu (1969) suggested a normalization scheme which collapses the mean-temperature vertical profile:

$$\theta(x_3) = \frac{|\langle \bar{T}(x_3) \rangle - \langle \bar{T}(x_3 = \frac{1}{2}) \rangle|}{\frac{1}{2}\Delta T}, \tag{25a}$$

$$\delta = 1/(2\,Nu). \tag{25b}$$

The model predictions of normalized mean temperature also collapse as shown in figure 7. Since the Nu is part of the normalization scheme and the model and experimental data give different values of Nu, the θ *versus* δ curve (calculated from model results) varies slightly, depending on whether the experimental or model value

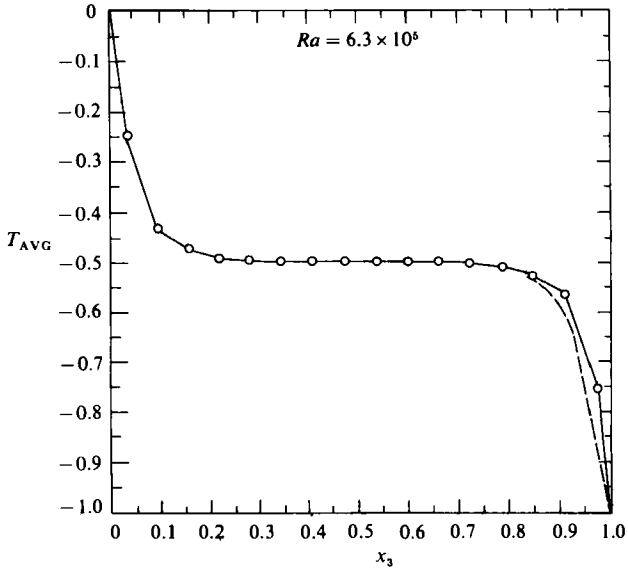

FIGURE 6. Horizontally averaged temperature profile: O—O, model; ---, Deardorff & Willis (1967).

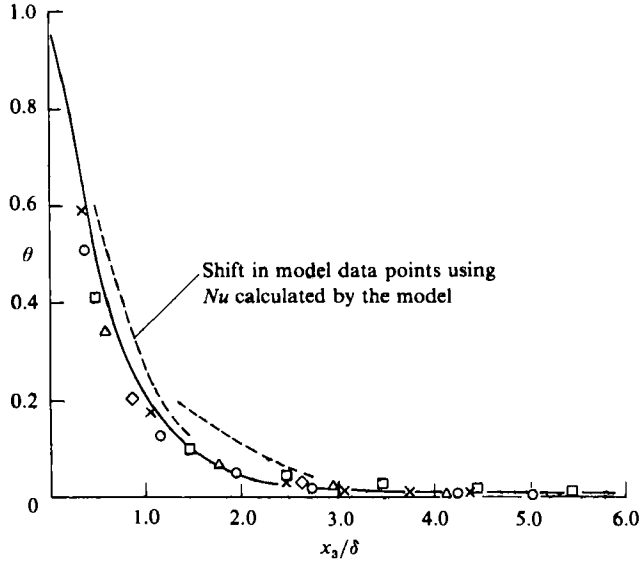

FIGURE 7. Normalized horizontally averaged temperature profile. Model: ×, $Ra = 3.8 \times 10^5$; O, 6.3×10^5; □, 1.4×10^6; △, 2.5×10^6; ◇, 1.0×10^7. ——, Goldstein & Chu.

of *Nu* for the same *Ra* is used. In both cases the data collapse; however, better quantitative agreement results from the use of the experimental value of *Nu* to normalize both the experimental and model mean temperature $\langle \overline{T}^t \rangle$. This is due to the fact that for the same *Ra* there is better agreement between $\langle \overline{T}^t \rangle$ than between *Nu* calculated and measured.

As mentioned previously, the grid resolution near the wall is a critical assumption in the overall model. As can be seen in figures 8–10, the model agrees reasonably well with the experimental results in the shape of the vertical-profile predictions of the

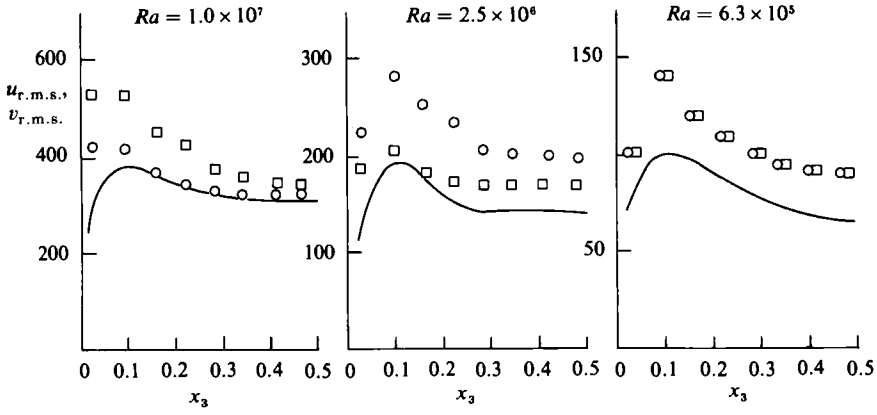

FIGURE 8. R.m.s. horizontal-velocity profile. Model: ○, $u_{\text{r.m.s.}}$; □, $v_{\text{r.m.s.}}$ ——, Deardorff & Willis (1967).

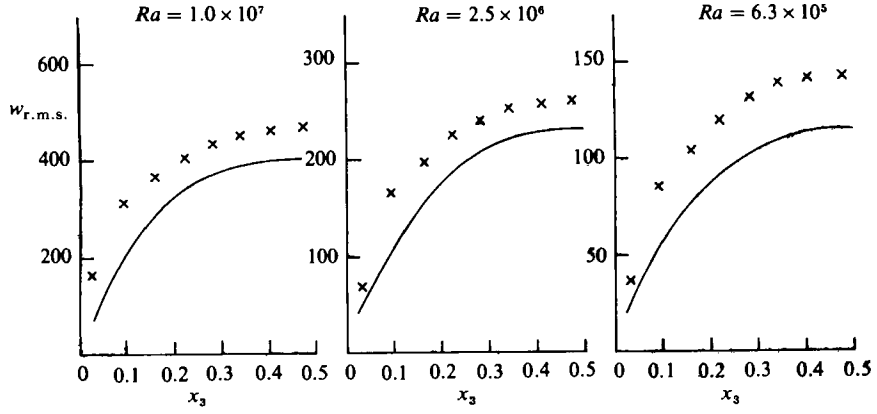

FIGURE 9. R.m.s. vertical velocity profile. Model: ×, $W_{\text{r.m.s.}}$ ——, Deardorff & Willis (1967).

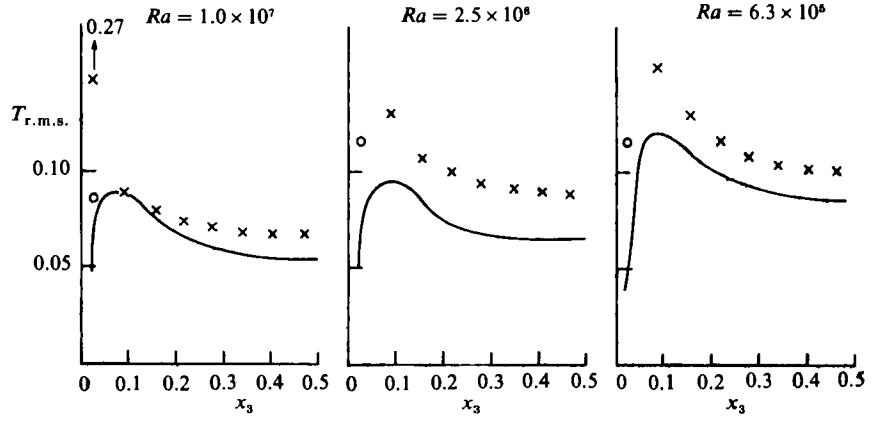

FIGURE 10. R.m.s. temperature profile. Model: ×, $T_{\text{r.m.s.}}$; ○, assumes $(T')_{\text{r.m.s.}}$ at $k = 1$ equals $(T')_{\text{r.m.s.}}$ at $k = 2$. ——, Deardorff & Willis (1967).

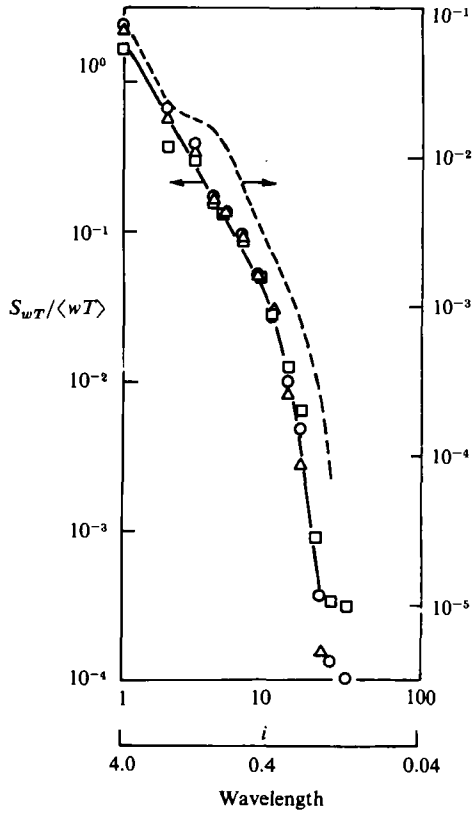

FIGURE 11. Co-spectra of vertical velocity and temperature. For model wavenumber = $\frac{1}{2}\pi i$. Model: □, $Ra = 1.0 \times 10^7$; ○, 2.5×10^6; △, 6.3×10^5. ---, Deardorff & Willis (1967).

r.m.s. velocity and temperature. The r.m.s. levels are high as was noted above. The only serious discrepancy occurs in the calculation of $T_{\text{r.m.s.}}$ at the grid point nearest to the wall. $T_{\text{r.m.s.}}$ is composed of a component calculated for the filtered field and one estimated for the subgrid field which is a function of $\partial\overline{T}^{\text{f}}/\partial x_3$. The estimated components were in serious error owing either to inaccuracies in $\partial\overline{T}^{\text{f}}/\partial x_3$ or in the derivation of the estimate as a result of the turbulence equilibrium assumption not being valid near the wall. When the subgrid estimate for the second grid point from the wall is used to calculate $T_{\text{r.m.s.}}$ next to the wall, the values are reasonable and the data plotted was calculated in this fashion. Note the subgrid component is a small part of the overall r.m.s. levels (at the Ra of this study) except for the erroneous calculations at grid point 1 and the above assumption should be reasonable.

Examples of the horizontal, one-dimensional spectra of the filtered velocity and temperature fields are shown in figures 11–13. The model data taken near the vertical centre has been time averaged to compare with the experimental results. They are compared with the data of Deardorff & Willis (1967). The experimental data were filtered using (8) and (9) and replotted. The model data were scaled differently from the results of Deardorff & Willis and have been plotted on a shifted axis in order to compare the slopes of the spectra. At the shorter wavelengths the model and the measurements compare favourably. At the longer wavelengths the effects of different aspect ratios prevent any detailed comparison. Owing to the low aspect ratio of the model, no peak in the spectra was observed. Such a peak should occur if the imposed

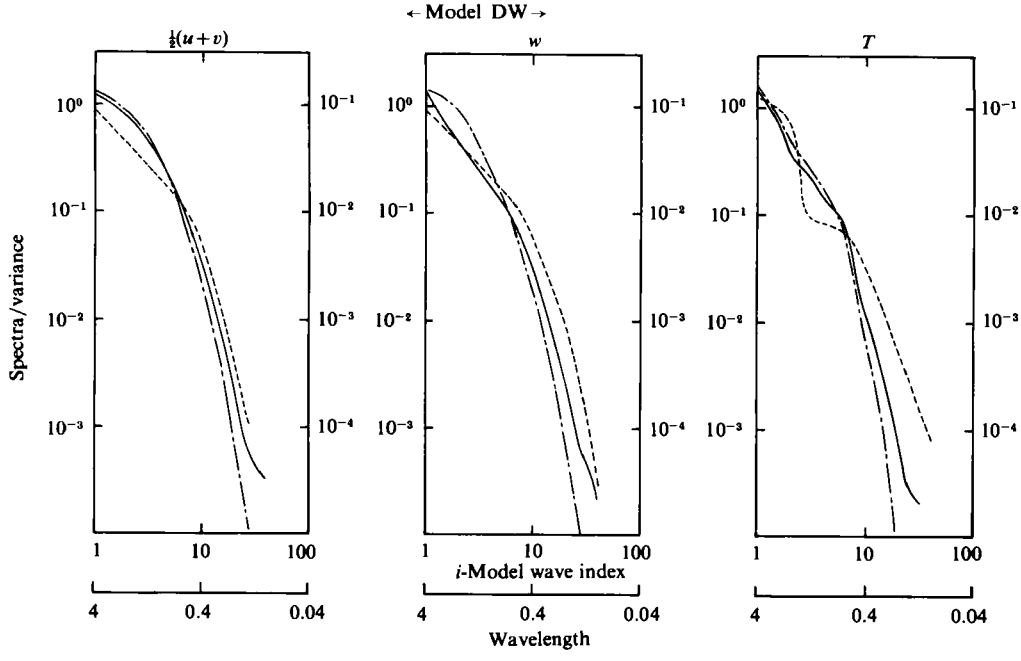

FIGURE 12. Spectra of $\frac{1}{2}(u+v)$, w and T. For model wavenumber $= \frac{1}{2}\pi i$. ——, Model $C = 0.21$; - - - - -, Deardorff & Willis (1967), filtered, $Ra = 2.5 \times 10^6$.

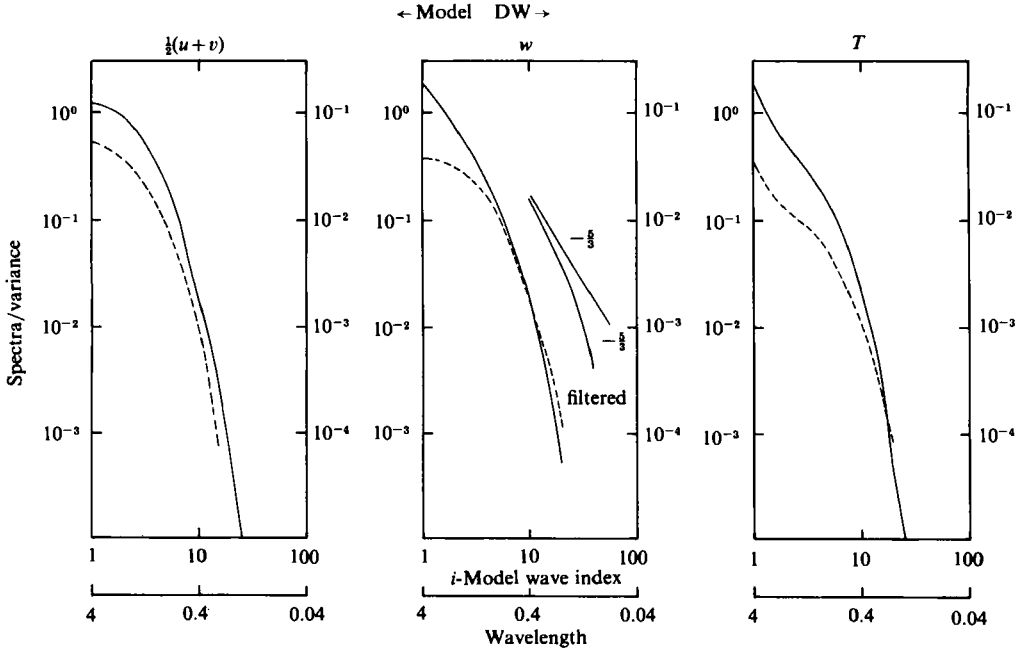

FIGURE 13. Spectra of $\frac{1}{2}(u+v)$, w and T. For model, wavenumber $= \frac{1}{2}\pi i$. ——, Model $C = 0.21$; - - - - -, Deardorff & Willis (1967), filtered, $Ra = 6.3 \times 10^5$.

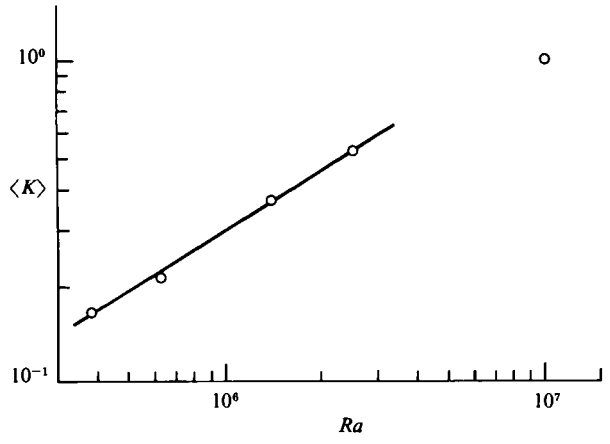

FIGURE 14. Turbulent viscosity/conductivity *vs* Ra, horizontal average at vertical centre.

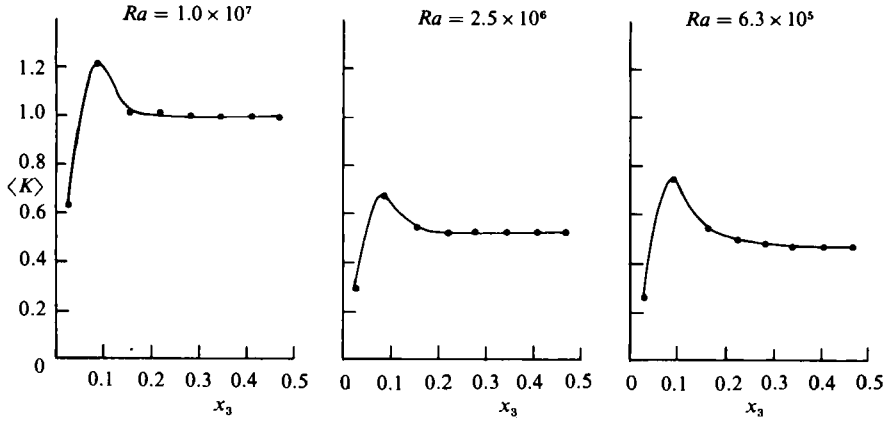

FIGURE 15. Turbulent viscosity/conductivity profile.

width of the horizontal boundary were large enough to allow the flow to select a characteristic flow length in the horizontal direction. In figure 13 a line with a slope of $-\frac{5}{3}$ has been filtered and drawn on the plot. At these values of Ra, a large equilibrium region does not occur (Deardorff & Willis 1967). The Reynolds number based on the Taylor microscale λ and the square root of the total kinetic energy ranges from $Re_\lambda = 28$ at $Ra = 3.8 \times 10^5$ to $Re_x = 90$ at $Ra = 1.0 \times 10^7$. λ was estimated as $(10\,Pr\,Pe^2/\epsilon)^{\frac{1}{2}}$ using a production-equals-dissipation assumption to estimate ϵ. Pe is the non-dimensional total kinetic energy.

An interesting output of the model is the amount of small-scale (subgrid) turbulence for the different values of Ra. The higher total turbulent production at the larger Ra should result in more subgrid turbulence. K is a measure of the subgrid turbulence level. Figure 14 shows the increase of K with Ra. K has been horizontally averaged at the vertical centre of the fluid layer. Figure 15 shows the variation of K away from the walls. This can be compared with the total turbulence production level P^* shown in figure 16. P^* is estimated as $Pr\,Ra\,\langle u_3 T \rangle$, where $\langle u_3 T \rangle$ is the horizontal average of the filtered and subgrid correlation between u_3 and T. The

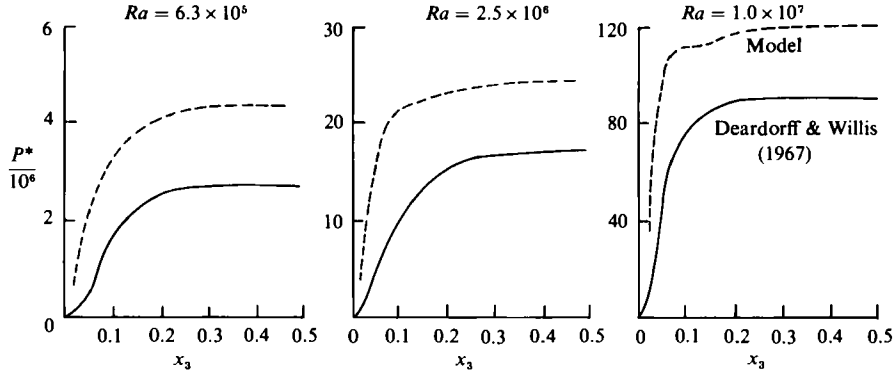

FIGURE 16. Comparison of the simulation model with experimental measurements, P^* *vs* z.

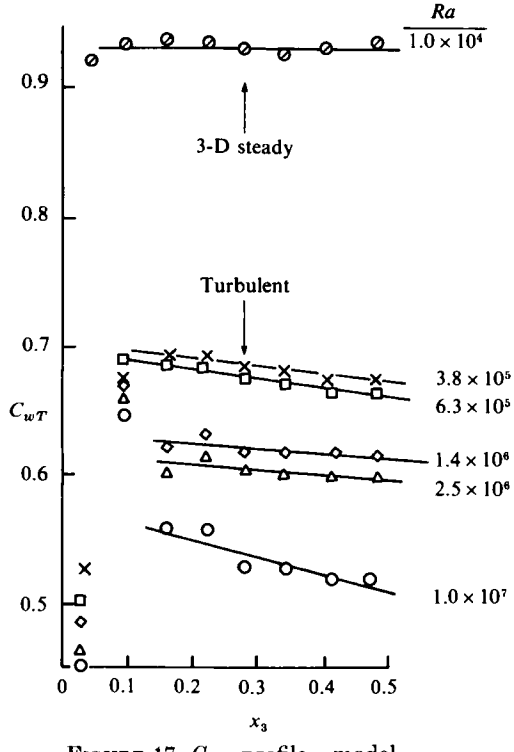

FIGURE 17. C_{wT} profile – model.

subgrid turbulent production P_{SG} is different from P^* and can be estimated from (13), (14), and (17) as follows,

$$P_{SG} \approx \epsilon \approx \text{constant} \times K^3. \tag{26}$$

Using figure 16, the variation in x_3 with P_{SG} can be compared with that for P^*. The integrals of P_{SG} and P^* across the fluid layer should both estimate the total turbulent production.

The correlation coefficient of the vertical velocity and temperature are plotted in figures 17 and 18. Since the correlation contains the subgrid estimates along with the filtered-field contribution and near the wall the subgrid estimates make a larger contribution, the coefficients must be viewed with caution in this region. Table 3

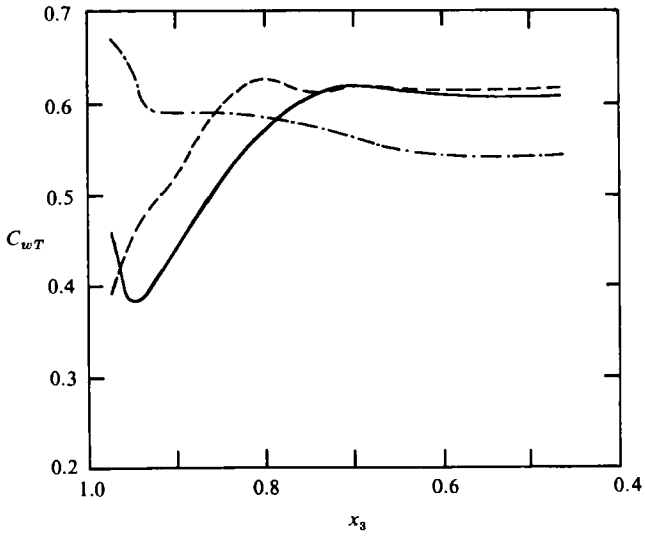

FIGURE 18. C_{wT} profile – Deardorff & Willis (1967): ——, $Ra = 6.3 \times 10^5$; – – –, 2.5×10^6; —·—, 1.0×10^7.

compares the levels from the computer model near the vertical centreline with several experimental values. Deardorff & Willis (1967) have measured the C_{wT} vertical profiles, and their data suggests the same slightly increasing negative slope with increasing Ra as is found in the model predictions. Near the wall neither the model nor the experiment are sufficiently accurate for detailed comparisons. The flat profile at $Ra = 10^4$ agrees with the direct-simulation results of Grotzbach (1982).

6.2. *Low-Rayleigh-number run*

When the subgrid model constant C is zero, the computer model will directly simulate the exact flow equations. One of the preliminary tests on the model was to run it with $C = 0$ and compare the results with other direct simulations. The agreement was satisfactory and the study reported in §6.1 was then conducted. The direct simulation was run for $Ra = 10^4$ and $Pr = 1$ with the boundary condition the same as for the study in §6.1. At these conditions the flow is not turbulent, but it is still of interest and so the results will be presented.

The model results were compared with a direct simulation by Hathaway (1982) who simulated the identical problem with a finite-difference code using a different numerical scheme. Also available for comparison were simulations by Lipps (1976) at $Ra = 9000$ and Grotzbach (1982) at $Ra = 7000$ but for $Pr = 0.76$. The present model predicted $Nu = 2.6$ ($A = 4$) compared with 2.4 ($A_x = 4.9$, $A_y = 6.0$) by Hathaway, 2.2 ($A_x = 4.0$, $A_y = 3.2$) by Lipps and 2.3 ($A = 2.8$) by Grotzbach. Interpolating the values of Lipps and Grotzbach to $Ra = 10^4$ gives $Nu = 2.3$ and 2.8 respectively. Experimental measurements give values several tenths lower (Grotzbach 1982), similar to the differences reported for high Ra. The model had a temperature-gradient reversal, $\partial T/\partial z = 0.08$, near the vertical centre of the fluid layer. The physical existence of such a temperature gradient has been debated in the literature but with no general consensus (Grotzbach 1982; and Chu & Goldstein 1973).

In figures 19 and 20, contour and vector plots of the velocity and temperature field are presented. No observable time changes were apparent after a stabilizing period

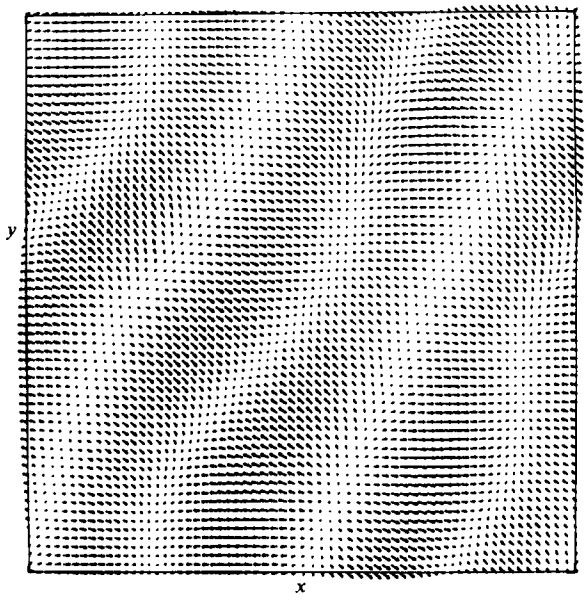

FIGURE 19. u, w vector plots at $Ra = 1.0 \times 10^4$.

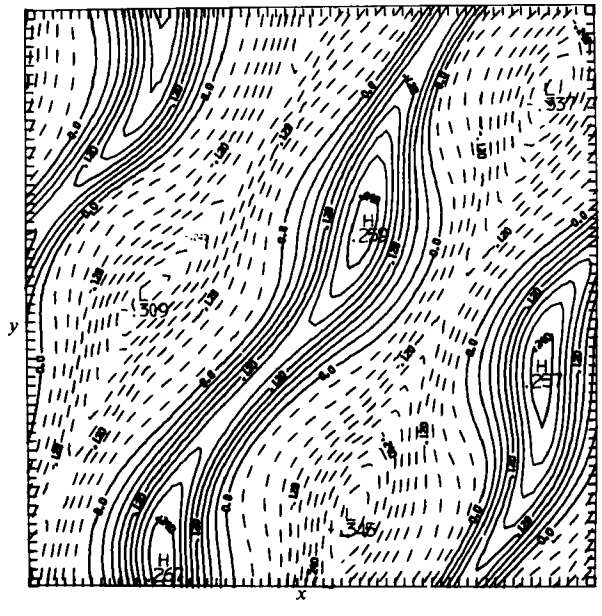

FIGURE 20. Temperature contour plot at $Ra = 1.0 \times 10^4$.

and thus the flow at only one time step is shown. The flow pattern of Hathaway was similar. The pattern was also observed by Grotzbach (1982) but for a lower $Ra = 4000$.

7. Conclusions

The overall results demonstrate that the LES technique can be used to simulate the physics in a turbulent-natural-convection problem. Resolution (which translates

to cost) is the major problem. Most work is needed in solving the resolution problem in the boundary region either through brute force (better computers and thus more grid points) or through a subgrid wall model. Use of a differential equation for the subgrid kinetic energy E_{SG} would help. E_{SG} could replace the velocity scale $\Delta_f \bar{S}^f$ used in (13*b*). A differential equation for E_{SG} could provide more flexibility and better assumptions in the subgrid model. In addition, improvements in the numerical technique could increase the accuracy of the calculation. A stretched grid with increased resolution near the walls is an obvious example. Pseudo-spectral techniques using either Tschebycheff or Legendre polynomials, combined implicit/explicit techniques and multi-grid techniques are currently being tested by the author and other researchers.

For more complicated flow geometries even improvements in computer hardware may not result in enough storage and speed to have sufficient grid points to resolve the flow in the inertial region of the energy spectrum. Models which account for the non-isotropic effects of the boundary conditions may then be necessary. This was the case in the present study near the wall. The LES of simple flows can be used to suggest and test such models by calculating the flow on a fine grid (with or without an equilibrium-based subgrid model) and comparing the results with a proposed model on a coarser grid (Clark *et al.* 1979). An extension of this idea leads one to a valuable use of the LES techniques, that is the evaluation of the terms in the long-time-averaged equations for the kinetic energy and Reynolds stresses. Since the large-scale flow is explicitly calculated, the spacial and temporal composition of these averaged terms can be studied. For example, the large-scale motion is buoyancy generated in the Rayleigh–Bénard problem. The smaller-scale motion is produced by the interaction of the larger-scale velocity field. A quantitative analysis of the flow scales, for which each of the above effects is important, could be calculated from the results of an LES.

The author would like to thank National Center for Atmospheric Research, Boulder, Colorado, and its sponsor, the National Science Foundation, for the computer resources and fellowship support used for this study. A special thanks goes to the Mesoscale Research Section of NCAR for the technical assistance that I received. The author gratefully acknowledges the conversations with Dr V. S. Arpaci, Dr J. R. Herring, Dr J. C. Wyngaard and Dr L. R. Scott.

REFERENCES

Antonopoulos-Domis, M. 1979 Aspects of large eddy simulation of homogeneous isotropic turbulence. *QMC EP* 6038, Department of Nuclear Engineering, Queen Mary College.

Businger, J. A. 1973 Turbulent transfer in the atmospheric surface layer. *Workshop in Micrometeorology*, p. 67. American Meteorology Society.

Busse, F. H. 1981 Transition to turbulence in Rayleigh–Bénard convection. In *Hydrodynamic Instabilities and the Transition to Turbulence* (ed. H. L. Swinney & J. P. Gollub). Springer.

Carroll, J. J. 1976 The thermal structure of turbulent convection. *J. Atmos. Sci.* **33**, 642.

Chandrasekhar, S. 1961 *Hydrodynamic and Hydromagnetic Stability*. Clarendon.

Chu, T. Y. & Goldstein, R. J. 1973 Turbulent convection in a horizontal layer of water. *J. Fluid Mech.* **60**, 141.

Clark, R. A., Ferziger, J. H. & Reynolds, W. C. 1979 Evaluation of subgrid-scale turbulence models using a fully simulated turbulent flow. *J. Fluid Mech.* **91**, 1.

Clever, R. M. & Busse, F. H. 1978 Large wavelength convection rolls in low Prandtl number fluids. *Z. angew. Math. Phys.* **29**, 711.

DEARDORFF, J. W. 1970*a* A numerical study of three-dimensional turbulent channel flow at large Reynolds numbers. *J. Fluid Mech.* **41**, 453.

DEARDORFF, J. W. 1970*b* Convection velocity and temperature scales for the unstable planetary boundary layer and for Rayleigh convection. *J. Atmos. Sci.* **27**, 1211.

DEARDORFF, J. W. 1971 On the magnitude of the subgrid scale eddy coefficient. *J. Comp. Phys.* **7**, 120.

DEARDORFF, J. W. 1972 Numerical investigation of neutral and unstable planetary boundary layers. *J. Atmos. Sci.* **29**, 91.

DEARDORFF, J. W. 1973 Three-dimensional numerical modeling of the planetary boundary layer. In *Workshop in Micrometeorology* (ed. D. A. Haugen), p. 271. American Meteorology Society.

DEARDORFF, J. W. & WILLIS, G. E. 1965 The effect of two-dimensionality on the suppression of thermal turbulence. *J. Fluid Mech.* **23**, 337.

DEARDORFF, J. W. & WILLIS, G. E. 1967 Investigation of turbulent thermal convection between horizontal plates. *J. Fluid Mech.* **28**, 675.

DENTON, R. A. & WOOD, I. R. 1979 Turbulent convection between two horizontal plates. *Intl J. Heat Mass Transfer* **22**, 1339.

EIDSON, T. M. 1982 Numerical simulation of the turbulent Rayleigh–Bénard problem using subgrid modeling. Ph.D. Thesis, University of Michigan.

FITZJARRALD, D. E. 1976 An experimental study of turbulent convection in air. *J. Fluid Mech.* **73**, 693.

GOLDSTEIN, R. J. & CHU, T. Y. 1969 Thermal convection in a horizontal layer of air. *Prog. Heat Transfer* **2**, 55.

GROTZBACH, G. 1980 Numerical simulation of turbulent temperature fluctuations in liquid metals. *Intl J. Heat Mass Transfer* **24**, 475.

GROTZBACH, G. 1982 Direct numerical simulation of laminar and turbulent Bénard convection. *J. Fluid Mech.* **119**, 27.

GROTZBACH, G. 1983 Spatial resolution for direct numerical simulation of the Rayleigh–Bénard convection. *J. Comp. Phys.* **49**, 241.

GROTZBACH, G. & SCHUMANN, U. 1979 Direct numerical simulation of turbulent velocity-, pressure- and temperature-fields in channel flows. In *Turbulent shear Flows I* (ed. F. Durst *et al.*), p. 370. Springer.

HATHAWAY, D. H. 1982 Nonlinear simulations of solar rotation effects in supergranules. *Solar Phys.* **77**, 341.

HERRING, J. R. 1979 Subgrid scale modeling – an introduction and overview. In *Turbulent Shear Flows I* (ed. F. Durst *et al.*), p. 347. Springer.

KRISHNAMURTI, R. 1970*a* On the transition to turbulent convection. Part 1. The transition from two- to three-dimensional flow. *J. Fluid Mech.* **42**, 295.

KRISHNAMURTI, R. 1970*b* On the transition to turbulent convection. Part 2. The transition to time-dependent flow. *J. Fluid Mech.* **42**, 309.

KWAK, D. 1975 Three-dimensional time dependent computation of turbulent flow. Ph.D. Thesis, Stanford University.

LILLY, D. K. 1962 On the numerical simulation of buoyant convection. *Tellus* **15**, 148.

LILLY, D. K. 1967 The representation of small-scale turbulence in numerical simulation experiments. In *Proc. of the IBM Scientific Computer Symposium on Environmental Sciences*, p. 195. IBM Form No. 320–1951.

LIPPS, F. B. 1976 Numerical simulation of three-dimensional Bénard convection in air. *J. Fluid Mech.* **75**, 113.

LIPPS, F. B. & SOMERVILLE, C. J. 1971 Dynamics of variable wave-length in finite-amplitude Bénard convection. *Phys. Fluids* **14**, 759.

LONG, R. R. 1976 Relation between Nusselt number and Rayleigh number in turbulent thermal convection. *J. Fluid Mech.* **73**, 445.

LONG, R. R. 1977 Some aspects of turbulence in geophysical systems. *Adv. Appl. Mech.* **17**, 1.

MCMILLAN, O. J. & FERZIGER, J. H. 1979 Direct testing of subgrid-scale models. *AIAA J.* **17**, 1340.

MANSOUR, N. N., MOIN, P., REYNOLDS, W. C. & FERZIGER, J. H. 1979 Improved methods for large eddy simulations of turbulence. In *Turbulent Shear Flows I* (ed. F. Durst *et al.*), p. 386. Springer.

MIHALJAN, J. M. 1962 A rigorous exposition of the Boussinesq approximation. *Astr. J.* **136**, 1126.

MOIN, P. & KIM, J. 1982 Numerical investigation of turbulent channel flow. *J. Fluid Mech.* **118**, 341.

MOIN, P., MANSOUR, N. N., REYNOLDS, W. C. & FERZIGER, J. H. 1978 Large eddy simulation of turbulent shear flow. Lecture Notes in Physics, Vol. 90. Springer.

PIACSEK, S. A. & WILLIAMS, G. P. 1970 Conservation properties of convection difference schemes. *J. Comp. Phys.* **6**, 392.

REYNOLDS, A. J. 1975 The prediction of turbulent Prandtl and Schmidt numbers. *Intl J. Heat Mass Transfer* **18**, 1055.

REYNOLDS, W. C. 1976 Computation of turbulent flows. *Ann. Rev. Fluid Mech.* **8**, 183.

ROBERT, A. J. 1966 The integration of a low order spectral form of the primitive meteorological equations. *J. Met. Soc. Japan* **44**, 237.

ROGALLO, R. S. & MOIN, P. 1984 Numerical simulation of turbulent flows. *Ann. Rev. Fluid Mech.* **16**, 99.

SCHUMANN, W. 1973 Ein Verfahren zur direckten numerischen Simulation turbulenter Stroemungen in Platten- und Ringspaltkanaelen und ueber seine Anwendung zur Untersuchung von Turbulenzmodellen. Thesis, Univesitaet Karlsruhe (NASA Technical Translation, *NASA TT F* 15, p. 391).

SCHUMANN, U., GROTZBACH, G. & KLEISER, L. 1980 Direct numerical simulation of turbulence. In *Prediction Methods for Turbulent Flows* (ed. W. Kollman), p. 124. Hemisphere.

SHAANAN, S. 1975 Numerical simulation of turbulence in the presence of shear. Ph.D. thesis, Stanford University.

SMAGORINSKY, J. 1963 General circulation experiments with the primitive equations. *Mon. Weather Rev.* **91**, 99.

SPIEGEL, E. A. & VERONIS, G. 1960 On the Boussinesq approximation for a compressible fluid. *Astrophys. J.* **131**, 442.

WILLIAMS, G. P. 1969 Numerical integration of the three-dimensional Navier–Stokes equations for incompressible flow. *J. Fluid Mech.* **37**, 727.